Analytical Methods

Accepted Manuscript

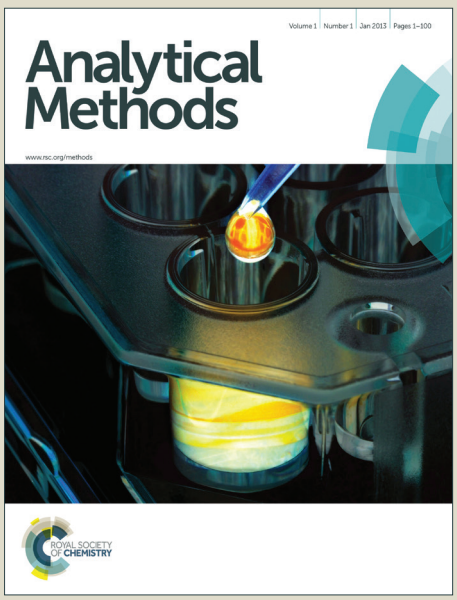

ROYAL SOCIETY OF CHEMISTRY

www.rsc.org/methods

Enhanced gas sensing performance of one-pot-synthesized Pt/$CdIn_2O_4$ composites with controlled morphologies

Chao Chen[a,b] Junhua Li[a,b] Riding Mi[a,b] Yanli Liu[a,b]*

[a] College of Material Science and Engineering, Hunan University, Changsha 410082, China

[b] Hunan Province Key Laboratory for Spray Deposition Technology and Application, Hunan University, Changsha 410082, China

*Corresponding Author: Yanli Liu, Email: yanliliu@hnu.edu.cn

Tel: 86-731-8882 1610; Fax: 86-731-8882 1610

Address: College of Materials Science and Engineering, Hunan University, Changsha 410082, China

Abstract: In this paper, Pt/$CdIn_2O_4$ composites with different morphologies and various Pt contents were prepared through a facile one-pot hydrothermal method. The crystallographic surface of $CdIn_2O_4$ crystals in different shapes, including octahedrons, truncated octahedrons, 14-facets polyhedrons and cubes were successfully controlled with different Pt contents. Inspired by the unique function of Pt and $CdIn_2O_4$, the Pt/$CdIn_2O_4$ composites were applied as gas-sensing materials. The tests of gas-sensing performance demonstrated that not only the Pt dopant but also the surface structure of $CdIn_2O_4$ crystals affected the gas-sensing properties of the samples obtained. $CdIn_2O_4$ with 0.98 at.% Pt exhibited the superior response to acetone, indicating a great potential application in gas sensors.

Keywords: $CdIn_2O_4$; Pt modification; Gas Sensor; Enhanced Performance

1. Introduction

The application of semiconductor metal oxides in the production of gas sensors has triggered much research activity because of their high response for different gaseous species [1-5]. The gas-sensing process of metal oxide sensors generally involves a catalytic reaction between the gas to be monitored and the adsorbed oxygen species on the surface of semiconductor metal oxides [6-10]. The particle size, defects, surface properties of metal oxides directly affect the state and the amount of adsorbed oxygen species and consequently the performance of the gas sensors. Different crystallographic facets corresponding to different shapes of metal oxides have distinctive surface atom structures and surface energies, which have been demonstrated in chemical reactivity, sensing property of nano- and microsized crystals [11-16]. Therefore, it is of great importance to predict and control the exposed facets and to explore the facet-dependent properties of metal oxides.

Besides the control over the morphologies of the metal oxides, surface modification by metals can also provide an alternative method to improve the sensor performance [17-27]. Nowadays, it is believed that the presence of catalytic noble metal elements, such as Au, Pt and Pd, on the surface of the metal oxides can enhance the sensing performance due to the good chare storage capability and the well-known spillover effect. For instance, it was found that in situ vapor deposition of Pd and Ag particles onto SnO_2 nanowires and nanobelts could enhance the gas sensing performance of SnO_2 materials [22, 23]. Especially, the metal oxide/metal hybrid

nanomaterials such as Au/ZnO nanopyramids [24], Ag/TiO_2 microspheres [25], Pd/ZnO nanowires [26], Pt/ZnO nanoflowers [27] have demonstrated great potential for application in gas sensors.

As a typical n-type semiconducting materials, cadmium indate ($CdIn_2O_4$) has received much attention over the past decade due to its unique optical and electronic properties [28-30]. Containing CdO and In_2O_3, that are the two good base materials of transparent conducting oxides [31], $CdIn_2O_4$ is characterized by its large energy separation between the first and second conduction bands and excellent electrical properties with a carrier concentration of about 1×10^{20} cm^{-3} without additional doping [32] and is expected to be an excellent gas sensing materials. Although the gas sensing properties of both $CdIn_2O_4$ thin films and $CdIn_2O_4$ nanoparticles have been studied [33, 34], the systematic investigation on the shape control of $CdIn_2O_4$ and the effect of Pt particles on the gas sensing properties of $CdIn_2O_4$ have not yet been accomplished.

In this study, $CdIn_2O_4$/Pt composites with different morphologies including octahedrons, truncated octahedrons, 14-facets polyhedrons, and cubes were fabricated via a fast one-step hydrothermal method. Furthermore, the sizes gradually decreased with the shape evolution of $CdIn_2O_4$ from octahedron to cube. Especially, the influences of the noble metal, Pt, on the gas-sensing properties of $CdIn_2O_4$ have been emphasized.

2. **Experimental section**

2.1 Materials synthesis

All of the reagents were analytical purity and were used without further purification. Cadmium nitrate ($Cd(NO_3)_2{\cdot}3H_2O$), indium nitrate ($In(NO_3)_3{\cdot}4.5H_2O$) and potassium hydroxide (KOH) were purchased from Beijing Chemical Reagent Company Limited of China. Hexachloroplatinic acid ($H_2PtCl_6{\cdot}6H_2O$) was obtained from Sinopharm Chemical Reagent Company Limited of China.

Typically, a aqueous solution of $Cd(NO_3)_2{\cdot}3H_2O$ was added to a aqueous solution of $In(NO_3)_3{\cdot}4.5H_2O$ at room temperature to form a clear solution with Cd/In molar ratio 1:1.8. A solution of KOH was added to the mixture with the molar ratios of the Cd^{2+}: In^{3+}: OH^- = 1:1.8:8 to form a white emulsion under stirring. The influence of molar ratio on the purity of $CdIn_2O_4$ has been discussed in our previous paper [35]. The emulsion was stirred for another 2 h. Then a suitable amount of $H_2PtCl_6{\cdot}6H_2O$ aqueous solution (0.02 g mL^{-1}) was added into the mixture. After further stirring for 1 h, the stock mixture was transferred into a 100 mL Teflon-lined stainless steel autoclave that was subsequently sealed and maintained at 260 °C for 20 h. After the reaction mixture had been cooled to room temperature naturally, the resulting precipitate was collected by centrifugation and washed several times with ethanol and deionized water alternately and dried at 70 °C in air for further characterization.

To evaluate the effect of Pt amount on the gas sensing properties of the base material, we have fabricated several types of devices with the increasing weight percent of Pt. The loading amount of Pt was denoted as *x* at.%, where *x* indicates the

percentage of Pt in the final products measured by an energy dispersive X-ray spectrometer (EDX).

2.2 **Materials characterizations**

The phases of the samples were characterized using X-ray diffraction (XRD; D/Max-2000 Rigaku) with Cu Kα radiation (λ = 0.15418 nm, 40 kV, 100 mA) at a scan rate of 8 °/min. The structural properties and morphology of the products were studied by field emission scanning electron microscopy (FESEM, Hitachi S-4800) with an accelerating voltage of 10 kV. energy dispersive X-ray (EDX) spectra were determined using the Hitachi S-4800 EDX spectrometer attached to field emission scanning electron microscopy. Transmission electron microscopy (TEM) images of the samples were taken at an accelerating voltage of 200 kV with a Tecnai F20 TEM.

2.3 Fabrication and measurement of gas sensor

The gas sensor structure and the testing method were similar to that of our previous reports [36, 37]. The gas sensor was fabricated by coating aqueous slurry of the synthesized samples onto the ceramic tube without an additional annealing process. Then a Ni-Cr alloy coil through the tube was employed as a heater to control the operating temperature, and the electrical contact was made through connecting the four platinum wires with the instrument base by gold paste. The gas sensing properties (sensor response and response/recovery curves) were performed on a computer controlled WS-30A (Weisheng Electronics Co. Ltd., China) system. Typically, the gas sensors were placed in a chamber and the gas sensing experiments were conducted under a pressure of 1 standard atmosphere and at relatively humidity

of 20%. Detecting gases were injected into the test chamber by a microinjector and were mixed with air by a little electric fan. The sensor was exposed to air again by removing the chamber. For reducing gases such as acetone, the gas response is determined as the ratio R_a/R_g, where R_a is the resistance in ambient air and R_g is the resistance in tested gas, respectively.

3. Results and discussion

3.1 Crystalline structure and morphology.

Fig. 1 (a-e) shows the typical morphologies of the sample obtained with different Pt amounts, from which we can see that all the $CdIn_2O_4$ particles are polyhedrons. The morphologies and sizes of $CdIn_2O_4$ change with the increase of Pt contents. The morphologies of $CdIn_2O_4$ vary from octahedron, corresponding to Pt = 0 at.% in Fig. 1a, to truncated octahedrons corresponding to Pt = 0.26 at.% in Fig. 1b, to 14-facets polyhedrons corresponding to Pt = 0.40 at.% in Fig. 1c, to microcubes corresponding to Pt = 0.98 at.% in Fig. 1d, and microcubes with smaller size corresponding to Pt = 1.75 at.% in Fig. 1e. From the images in Fig. 1(a-e), it is also obvious that the size is smaller and smaller with the increment of Pt amount. Corresponding EDX spectra, shown in Fig. 1(a'-e'), confirm that the samples consist primarily of Cd, In, O for pristine $CdIn_2O_4$ and Cd, In, O, Pt for Pt/$CdIn_2O_4$, respectively.

The crystal phase of Pt/$CdIn_2O_4$ with different loading amounts of Pt was characterized by X-ray powder diffraction. As shown in Fig. 2a, the sharp diffraction peaks indicate the good crystalline quality of $CdIn_2O_4$ when the weight percent of Pt

was 0 at.%. The XRD pattern shows peaks at 16.7°, 27.5°, 32.3°, 33.8°, 39.2°, 48.6°, 51.8°, 56.8°, 59.6°, 64.2°, 66.9°, 67.7°, 71.2°, and 77.9° indexed to (111), (220), (311), (222), (400), (422), (511), (440), (531), (620), (533), (622), (444), and (642) planes of the $CdIn_2O_4$ crystal given by the standard data file (JCPDS No. 29-0258). $CdIn_2O_4$ crystals are of cubic spinel structure with lattice constant a = 9.166 nm. There are no other clear peaks coincident with those peaks of impurities. By comparison, it is observed that the XRD patterns of Pt/$CdIn_2O_4$, Fig. 2(b-e), are very similar to that of the pure one, indicating that the formation of Pt in the hydrothermal reaction process has no influence on the crystal structure of $CdIn_2O_4$. There are almost no diffraction peaks of Pt in the XRD pattern when the Pt amount is as low as 0.26 at.% (Fig. 2b), which can be explained by consider that the quantity of Pt is much smaller than that of $CdIn_2O_4$. With increasing weight percent of Pt, 0.40 at.%, 0.98 at.% and 1.75 at.%, the peaks indexed to Pt at 39.8°, 46.2°, which can be ascribed to the (111), (200) planes of face-centered cubic (fcc) Pt (JCPDS No. 04-0802), also appear and the intensities of those peaks increase gradually, indicating more and more Pt particles are attached on the $CdIn_2O_4$ (Fig. 2c, 2d, 2e).

Fig. 3a is a TEM image of $CdIn_2O_4$ particles loaded with 0.98 at.% Pt, clearly showing their microcube morphology with sizes of about 120 nm. $CdIn_2O_4$ has an FCC cubic structure and the exposed surfaces of the cubes are made of six {100} facets. As shown in Fig 3b, two well-faceted cubic particles under an electron beam perpendicular to their top surface resemble squares. Fig. 3c is a high-resolution TEM (HR-TEM) image showing the interface between Pt and $CdIn_2O_4$. The contrast

difference between Pt and $CdIn_2O_4$ is apparent. HRTEM image reveals the clear parallel fringes with d-spacing of 0.324 nm, which corresponds to {220} crystal planes of $CdIn_2O_4$. The interplannar distance of 0.227 nm corresponds to Pt (111) planes. Fig. 3d contains the corresponding electron diffraction patterns of Pt-$CdIn_2O_4$ in TEM apparatus, showing two different natures of crystals. One set of diffraction patterns with a square symmetry, which is the typical diffraction pattern of the [001] zone axis, can be indexed to single-crystal $CdIn_2O_4$, and the other irregular diffraction spots (marked with white arrows) arise from the small-sized Pt nanoparticles.

3.2 Formation mechanism of the morphology

SEM observation of the samples reveals that the shape and size of the as-prepared $CdIn_2O_4$ polyhedral particles depend closely on the addition of Pt. As the amount of Pt increases, the morphologies of the samples change from octahedron to cube with the decreasing size. Pt particles was derived from the reduction of precursor, $H_2PtCl_6 \cdot 6H_2O$. Hexachloroplatinic acid is a weak acid and it has acidic character to affect the pH value of the whole reaction. In fact, the growth of $CdIn_2O_4$ is related to the specific pH value of the system. Previous investigations confirmed that OH^- was a successful capping agent for different crystals [38-40]. As for the samples corresponding to different amount of Pt in this work, measurements of the pH value of the reaction system before and after the hydrothermal experiments showed the changed acidity and detailed pH information is summarized in Table 1. As we can see, before the addition of $H_2PtCl_6 \cdot 6H_2O$ aqueous solution, the original pH value of the system was 12.46. There was a chemical reaction of the OH^- with the metal cations

during the hydrothermal process which could generate insoluble final product, resulting in decrease of pH value, 9.23. With the increase of the Pt precursor, pH values appeared decreasing gradually. Therefore, it could be concluded that the modification of Pt with various content might modulate the OH^- content and further modulate the morphology of the final products.

3.3 Gas sensing properties

It is well known that morphology, size, and surface structure of metal oxide semiconductor can dramatically change its gas-sensing performance [41, 42]. The deposition of noble metal particles onto the metal oxide has also been demonstrated to improve the gas-sensing properties [26, 27]. So, it could be expected that such a $CdIn_2O_4$ modified by Pt particles might be a potential candidate for gas sensing applications. First, the sensors based on $CdIn_2O_4$ modified by different amount of Pt were performed at different operating temperatures to 100 ppm of acetone. The optimal operating temperature seems to correlate with the activation energy barrier related to testing gases [43]. The sensor response as a function of the operating temperatures from 150 to 420 ℃ is shown in Fig. 4, which indicates that the response of the sensors increase and reach maximum at 270 °C and then decrease rapidly with further increase of operating temperature. From Fig. 4, other important information could also be obtained. Compared with the pristine $CdIn_2O_4$, the gas sensing performance of Pt/$CdIn_2O_4$ to acetone increases with the increment of Pt amount, up to 0.98 at.%, and decreases with further increment of Pt amount. $CdIn_2O_4$ modified by 1.75 at.% Pt leads to poor responses maybe because too much Pt particles blott out the

active sites of $CdIn_2O_4$ and cause a decrease of the adsorbed oxygen and finally a poor response of acetone.

A comparison of the response/recovery performance of the sensors based on $CdIn_2O_4$ and Pt/$CdIn_2O_4$ as a function of acetone concentrations at the working temperature of 270 °C is presented in Fig. 5a. It can be seen that the response of $CdIn_2O_4$ based sensor gradually increases as the acetone concentrations increase from 10 to 200 ppm, which demonstrates that $CdIn_2O_4$ based sensor has a wide detection limit for acetone. The sensor based on $CdIn_2O_4$ modified by Pt shows much higher response than the pristine $CdIn_2O_4$ sensor. The relations between sensor response and gas concentration are shown in Fig.5b. The linear relationships between the responses and the gas concentrations suggest that the sensor response exhibits a good dependence on the gas concentration.

Such good performances can be attributed to the contribution of the gas-sensing reactivity on crystal facets in different orientations of $CdIn_2O_4$ and the interface between $CdIn_2O_4$ and Pt particles. In what follows, the possible contribution is discussed in two sections. The first is dealing with the adsorption/desorption phenomena and reactions at the surface. The second describes the possible chemical influence of the catalytic activity of Pt particles in the region close to the interface.

$CdIn_2O_4$ is an n-type semiconductor. According to Wolkenstein's model for semiconductor [44, 45], exposure of the $CdIn_2O_4$ sensor to air results in O_2 adsorption on the $CdIn_2O_4$ surface, which traps electrons from the conduction band of semiconductor to form oxygen species (O_2^-, O^-, O^{2-}). When a kind of reductive gas,

for example, acetone, is introduced, the reductive gas would react with the adsorbed oxygen species, which leads to a relatively strong activation on the surface of the $CdIn_2O_4$ sensor. Therefore, surface accessibility is crucial to maintain the high response of the crystals. From a crystallographic point of view, $CdIn_2O_4$ is a structure of spinel oxides, forming face-centered-cubic (FCC) closed packing. As an FCC crystal, a general sequence of surface energies may hold, $\gamma\{111\} < \gamma\{100\} < \gamma\{110\}$ [46]. The cubic $CdIn_2O_4$ may have a larger active surface area of {100} facets than the octahedral, which can provide more active space for the interaction between $CdIn_2O_4$ and the detected gases and thus demonstrates a higher response.

The chemical effects of the Pt/$CdIn_2O_4$ interface are related to the catalytic nature of Pt. By the assistance of Pt, oxygen molecules can be more easily adsorbed on the surface of $CdIn_2O_4$. Because Pt is a far better oxygen dissociation catalyst than $CdIn_2O_4$, adsorbed oxygen can diffuse faster to surface vacancies and capture electrons from the conduction band of $CdIn_2O_4$ to become oxygen ions. This process increases both the quantity of adsorbed oxygen and the molecule-ion conversion rate. Furthermore, because Pt can break hydrocarbons into more active radicals due to the catalysis, the production of the reaction between surface adsorbed oxygen ions and reducing gases is increased. At the regions close to the Pt/$CdIn_2O_4$ interface, the electrons are released more easily from the surface reaction back into the conduction band of $CdIn_2O_4$, which greatly increases the conductivity of Pt/$CdIn_2O_4$ in reducing gas ambience. Thus, these regions close to the Pt/$CdIn_2O_4$ interface make the sensors more active in gas detection.

4. Conclusion

In summary, $CdIn_2O_4$ with different polyhedral shape modified by Pt particles was synthesized in one step by a convenient and low-temperature hydrothermal process without further heat treatment. The changing trend of $CdIn_2O_4$ shape changed from regular octahedral to truncated octahedral, 14-faceted polyhedral, and then regular cubic. In addition, gas sensors based on polyhedral $CdIn_2O_4$ exhibited high response to acetone. The cubic $CdIn_2O_4$ showed distinctly greater response than the other because of their exposed active facets and the catalytic activity of Pt particles.

Acknowledgement

This work was financially supported by the National Natural Science Foundation of China (No.61404046), Fundamental Research Funds for the Central Universities (No. 531107040415), the Science and Technology Planning Project of Hunan Province, China (No. 2014GK3093).

References

[1] G. Korotcenkov, Metal oxides for solid-state gas sensors: What determines our choice? Mater. Sci. Eng. B. 139 (2007) 1-23.

[2] Y.F. Sun, S.B. Liu, F.L. Meng, J.Y. Liu, Z. Jin, L.T. Kong, J.H. Liu, Metal oxide nanostructures and their gas sensing properties: a review, Sensors, 12 (2012) 2610-2631.

[3] Y.F. Cao, Z.X. Cheng, J.Q. Xu, Y. Zhang, Q.Y. Pan, $CdSnO_3$ micro-cubes with porous architecture: synthesis and gas-sensing properties, CrystEngComm, 11 (2009) 2615-2617.

[4] Y.J. Chen, L.Yu, D. Feng, M. Zhuo, M. Zhang, E.D. Zhang, Z. Xu, Q.H. Li, T.H. Wang, Superior ethanol-sensing properties based on Ni-doped SnO_2 p-n heterojunction hollow spheres, Sens. Actuators B, 166-167 (2012) 61-67.

[5] Y. Zhang, J.Q. Xu, Q. Xiang, H. Li, Q.Y. Pan, P.C. Xu, Brush-like hierarchical ZnO nanostructures: synthesis, photoluminescence and gas sensor properties, J. Phys. Chem. C, 113 (2009) 3430-3435

[6] A.J.T. Naik, M.E.A. Warwick, S.J.A. Moniz, C.S. Blackman, I.P. Parkin, R. Binions, Nanostructured tungsten oxide gas sensors prepared by electric field assisted aerosol assisted chemical vapor deposition, J. Mater. Chem. A, 1 (2013) 1827-1833.

[7] X.Z. Wang, W. Liu, J.R. Liu, F.L. Wang, J. Kong, S. Qiu, C.Z. He, L.Q. Luan, Synthesis of nestlike ZnO hierarchically porous structures and analysis of their gas sensing properties, Appl. Mater. Interfaces, 4 (2012) 817-825.

[8] J.C. Chen, J.Q. Xu, SnO_2-based R134a gas sensor: sensing materials preparation, gas

response and sensing mechanism, Sens. Actuators B, 157 (2011) 494-499.

[9] Y. Zeng, T. Zhang, H.T. Fan, W.Y. Fu, G.Y. Lu, Y.M. Sui, H.B. Yang, One-pot synthesis and gas-sensing properties of hierarchical $ZnSnO_3$ nanocages, J. Phys. Chem. C, 113 (2009) 19000-19004.

[10] T .Kida, T. Doi, K. Shimanoe, Synthesis of monodispersed SnO_2 nanocrystals and their remarkably high sensitivity to volatile organic compounds, Chem. Mater., 22 (2010) 2662-2667.

[11] X.G. Han, M.S. Jin, S.F. Xie, Q. Kuang, Z.Y. Jiang, Y.Q .Jiang, Z.X. Xie, L.S. Zheng, Synthesis of tin dioxide octahedral nanoparticles with exposed high-energy {221} facets and enhanced gas-sensing properties, Angew. Chem. Int. Ed., 48 (2009) 9180-9183.

[12] B.Y. Geng, C.H. Fang, F M. Zhan, N. Yu, Synthesis of polyhedral $ZnSnO_3$ microcrystals with controlled exposed facets and their selective gas-sensing properties, Small, 4(2008) 1337-1343.

[13] L.X. Han, J. Liu, Z.J. Wang, K. Zhang, H. Luo, B. Xu, X. Zou, X. Zheng, B. Ye, X.B. Yu, Shape-controlled synthesis of $ZnSn(OH)_6$ crystallites and their HCHO-sensing properties, CrystEngComm, 14 (2012) 3380-3386.

[14] Y.Q. Jiang, X.X. Chen, R. Sun, Z. Xiong, L.S. Zheng, Hydrothermal syntheses and gas sensing properties of cubic and quasi-cubic Zn_2SnO_4, Mater. Chem. Phys., 129 (2011) 53-61.

[15] A.Gurlo, Nanosensors: does crystal shape matter? Small, 6 (2010) 2077-2079.

[16] S. Cho, J.W. Jang, J.S. Lee, K.H. Lee, Exposed crystal face controlled synthesis of 3D

ZnO superstructures, Langmuir, 26 (2010) 14255-14262.

[17] W. Wei, Y. Dai, B.B. Huang, Role of Cu doping on SnO_2 sensing properties toward H_2S, J. Phys. Chem. C, 115 (2011) 18597-18602.

[18] Q. Xiang, G.F. Meng, H.B. Zhao, Y. Zhang, H. Li, W.J. Ma, J.Q. Xu, Au nanoparticle modified WO_3 nanorods with their enhanced properties for photocatalysis and gas sensing, J. Phys. Chem. C, 114 (2010) 2049-2055.

[19] H.H. Wang, Z.H. Sun, Q.H. Lu, F.W. Zeng, D.S. Su, One-pot synthesis of (Au-nanorod)-(metal sulfide) core-shell nanostrucutres with enhanced gas-sensing property, Small, 8 (2012) 1167-1172.

[20] V. Subramanian, E.E. Wolf, P.V. Kamat, Catalysis with TiO_2/gold nanocomposites. Effect of metal particle size on the Fermi level equilibration, J. Am. Chem. Soc., 126 (2004), 4943-4950.

[21] J. Geng, G.H. Song, X.D. Jia, F.F. Cheng, J.J. Zhu, Fast-one-step synthesis of biocompatible ZnO/Au nanocomposites with hollow doughnut-like and other controlled morphologies, J. Phys. Chem. C, 116 (2012) 4517-4525.

[22] A. Kolmakov, D.O. Klenov, Y. Lilach, S. Stemmer, M. Moskovits, Enhanced gas sensing by individual SnO_2 nanowires and nanobelts functionalized with Pd catalyst particles, Nano Lett., 5 (2005) 667-673.

[23] X.Y. Xue, Z.H. Chen, C.H. Ma, L.L. Xing, Y.J. Chen, Y.G. Wang, T.H. Wang, One-step synthesis and gas-sensing characteristics of uniformly loaded Pt@SnO_2 nanorods, J. Phys. Chem. C, 114 (2010) 3968-3972.

[24] X.J. Wang, W. Wang, Y.L. Liu, Enhanced acetone sensing performance of Au

nanoparticles functionalized flower-like ZnO, Sens. Actuators B, 168 (2012) 39-45.

[25] X.L. Cheng, Y.M.Xu, S. Gao, H. Zhao, L.H. Huo, Ag nanoparticles modified TiO_2 spherical heterostructures with enhanced gas-sensing performance, Sens. Actuators B, 155 (2011) 716-721.

[26] Y. Zhang, J.Q. Xu, P.C. Xu, Y.H. Zhu, X.D. Chen, W.J. Yu, Decoration of ZnO nanowires with Pt nanoparticles and their improved gas sensing and photocatlytic performance, Nanotechnology, 21 (2010) 285501-285507.

[27] L.L. Xing, C.H. Ma, Z.H. Chen, Y.J. Chen, X. Yu, High gas sensing performance of one-step-synthesized Pd-ZnO nanoflowers due to surface reactions and modifications, Nanotechnology, 22(2011) 215501-215507.

[28] F. Yang, L. Fang, S. Zhang, K. Liao, G. Liu, J. Dong, L. Li and G. Fu, Optical properties of $CdIn_2O_4$ thin films prepared by DC reactive magnetron sputtering, J. Cryst. Growth, 297 (2006) 411-418.

[29] J. Yu, B. Huang, Z. Wang, X. Qin, X. Zhang, P. Wang, Self-template synthesis of $CdIn_2O_4$ hollow spheres and effects of Cd/In molar ratios on its morphologies, Inorg. Chem., 48 (2009) 10548-10552.

[30] A. Walsh, J.L.F. Da Silva, S.H. Wei, Multi-component transparent conducting oxides: progress in materials modeling, J. Phys.: Condens. Matter., 23 (2011), 334210(1)-334210(22).

[31] A. Bouhemadou, R. Khenata, D. Rached, F. Zerarga, M. Maamache, Structural, electronic and optical properties of spinel oxides: cadmium gallate and cadmium indate, Eur. Phys. J. Appl. Phys., 38 (2007) 203-210.

[32] P.P. Edwards, A. Porch, M.O. Jones, D.V. Morgan, R.M. Perks, Basic materials physics of transparent conducting oxides, Dalton Trans., 19 (2004) 2995-3002.

[33] Y. Dong, W. Wang, K. Liao, Ethanol-sensing characteristics of pure and Pt-activate $CdIn_2O_4$ films prepared by R.F. reactive sputtering, Sens. Actuators B, 67 (2000) 254-257.

[34] M. Cao, Y. Wang, T. Chen, M. Antonietti, M. Niederberger, A highly sensitive and fast-responding ethanol sensor based on $CdIn_2O_4$ nanocrystals synthesized by a nonaqueous sol-gel route, Chem. Mater., 20 (2008) 5781-5786.

[35] Y.L. Liu, C. Kong, X.J. Lü, F.H. Liao, F.Q. Huang, J.H. Lin, One-step hydrothermal synthesis of high-performance gas-sensing crystals $CdIn_2O_4$ with octahedral shape, Cryst. Growth Des., 12 (2012) 4104-4108.

[36] Y.L. Liu, H.F. Yang, Y. Yang, Z.M. Liu, G.L. Shen, R.Q. Yu, Gas sensing properties of tin dioxide coated onto multi-walled carbon nanotubes, Thin Solid Films, 497 (2006) 355-360.

[37] Y.L. Liu, Z.M. Liu, Y. Yang, H.F. Yang, G. Shen, R.Q. Yu, Simple synthesis of $MgFe_2O_4$ nanoparticles as gas sensing materials, Sens. Actuators B, 107 (2005) 600-604.

[38] H. Yu, R.Y. Lai, H.Q. Zhuang, Z.Z. Zhang, X.X. Wang, Controllable synthesis of crystallographic facet-oriented polyhedral $ZnSn(OH)_6$ microcrystals with assistance of a simple ion, CrystEngComm, 14 (2012) 8530-8535.

[39] J.Z. Yin, F. Gao, C.Z. Wei, Q.Y. Lu, Controlled growth and applications of complex metal oxide $ZnSn(OH)_6$ polyhedra, Inorg. Chem.,51 (2012) 10990-10995.

[40] X.J. Yu, H.X. Lu, Q. Li, Y.L. Zhao, L.W. Zhang, B.B. Fan, D.L. Chen, H.L. Wang, H.L. Xu, R. Zhang, Hydrothermal synthesis and characterization of micro/nanostructured $ZnSn(OH)_6$/ZnO composite architectrures, Cryst. Res. Technol., 46 (2011) 1175-1180.

[41] M.J.S. Spencer, I. Yarovsky, ZnO nanostrucutres for gas sensing: interaction of NO_2, NO, O, and N with the ZnO (1010) surface, J. Phys. Chem. C, 114 (2010) 10881-10893.

[42] J.Q. Xu, X.H. Jia, X.D. Lou, G.X. Xi, J.J. Han, Q.H. Gao, Selective detection of HCHO gas using mixed oxides of ZnO/$ZnSnO_3$, Sens. Actuators B, 120 (2007) 694-699.

[43] Z.J. Wang, J. Liu, F.J. Wang, S.Y. Chen, H. Luo, X.B. Yu, Size-controlled synthesis of $ZnSnO_3$ cubic crystallites at low temperatures and their HCHO-sensing properties, J. Phys. Chem. C, 114 (2010) 13577-13582.

[44] H. Haick, M. Ambrico, T. Ligonzo, R.T. Tung, D. Cahen, Controlling semiconductor/metal junction barriers by incomplete, nonideal molecular monolayers, J. Am. Chem. Soc., 128 (2006) 6854-6869.

[45] S. Gomri, J.L. Seguin, J. Guerin, K. Aguir, Adsorption-desorption noise in gas sensors: Modelling using Langmuir and Wolkenstein models for adsorption, Sensors Actuators B, 114(2006) 451-459.

[46] Z.L. Wang, Transmission electron microscopy of shape-controlled nanocrystals and their assemblies, J. Phys. Chem. B, 104(2000) 1153-1175.

Figure captions

Fig. 1 SEM images and corresponding EDS spectra of $CdIn_2O_4$ with different weight percent of Pt: (a, a') 0 at.%; (b, b') 0.26 at.%; (c, c') 0.40 at.%; (d, d') 0.98 at.%; (e, e') 1.75 at.%.

Fig. 2 XRD patterns of the $CdIn_2O_4$ and $Pt/CdIn_2O_4$ with different weight percent of Pt: (a) 0 at.%; (b) 0.26 at.%; (c) 0.40 at.%; (d) 0.98 at.% (e) 1.75 at.%.

Fig. 3 TEM images (a, b), HRTEM image (c), corresponding electron diffraction patterns (d) of $CdIn_2O_4$ modified by 0.98 at.% Pt.

Fig.4 The responses of $Pt/CdIn_2O_4$ with various Pt contents to 100 ppm of acetone at different operating temperature.

Fig.5 (a) Response and recovery curves of $Pt/CdIn_2O_4$ with various Pt contents to acetone with increasing concentrations at operating temperature of 270 °C; (b) Calibration curves of the sensor to acetone.

Table 1 The pH values of the system with different amount of Pt precursor before and after the hydrothermal experiments.

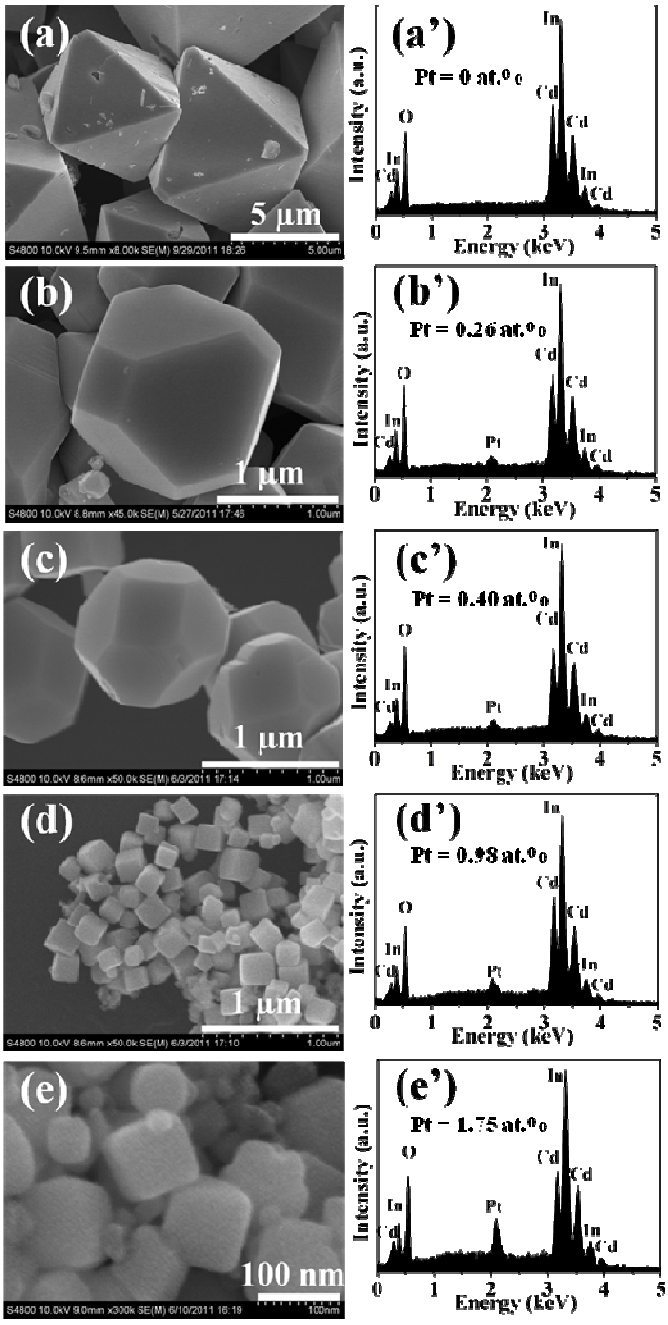

Fig. 1

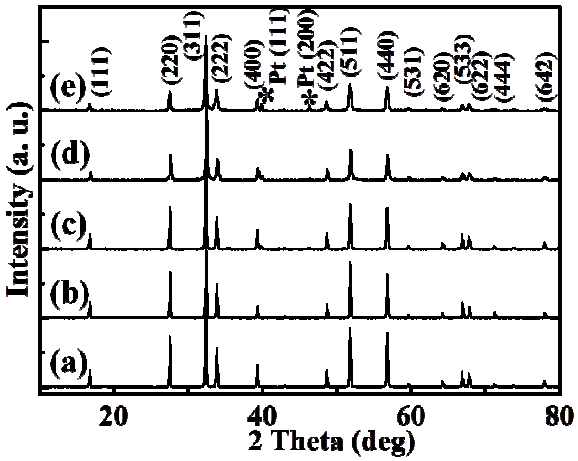

Fig. 2

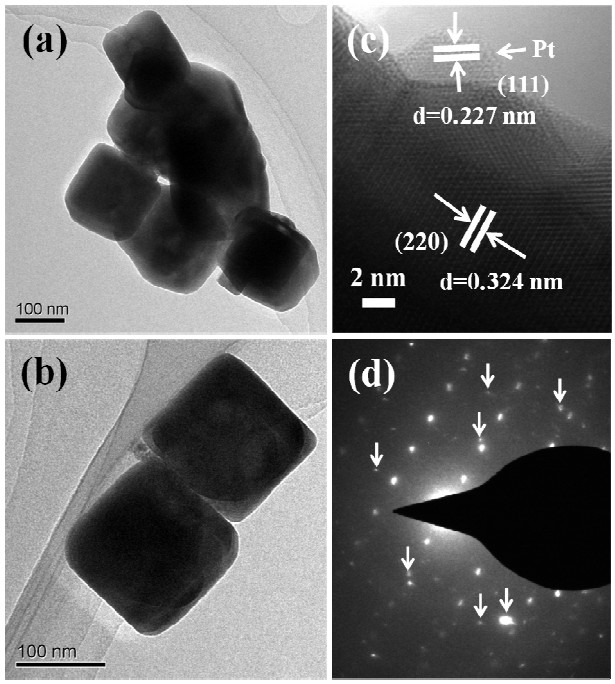

Fig. 3

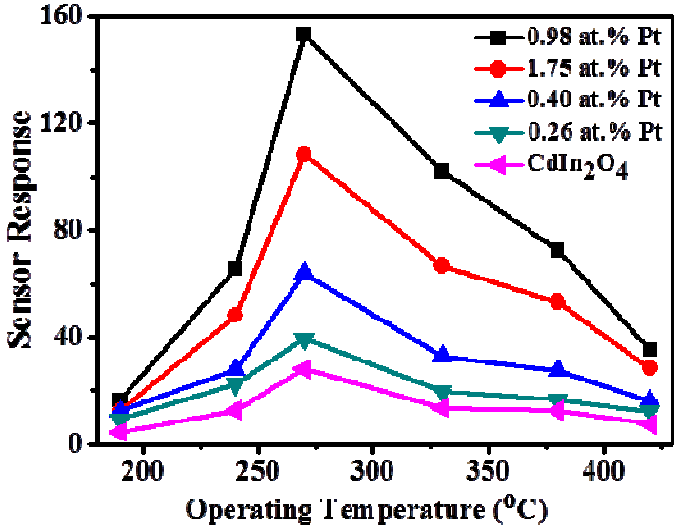

Fig. 4

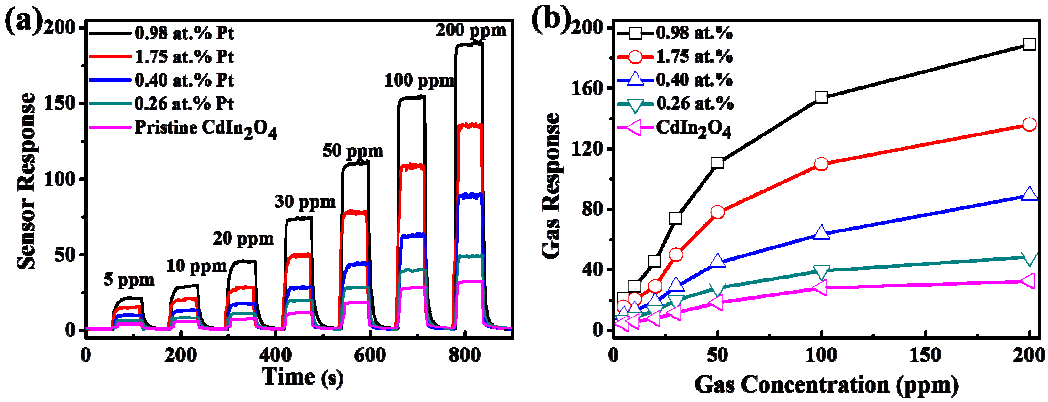

Fig. 5

Table 1

Pt Contents	pH Value of the System Before the Hydrothermal Experiments	pH Value of the System after the Hydrothermal Experiments
0 at.%	12.46	9.23
0.26 at.%	11.76	8.36
0.40 at.%	10.35	8.18
0.98 at.%	9.63	7.36
1.75 at.%	9.21	7.14